International Journal of Nanomedicine Dovepress

Open Access Full Text Article ORIGINAL RESEARCH

Exenatide-Modified Deferoxamine-Based Nanoparticles Ameliorates Neurological Deficits in Parkinson's Disease Mice

Yiming Huang[1,*], Xinran Wang[1,*], Wenjing Li[1,*], Feng Yue[1,2], Miao Wang[1], Feifan Zhou[1,2]

[1]State Key Laboratory of Digital Medical Engineering, School of Biomedical Engineering, Hainan University, Sanya, People's Republic of China; [2]One Health Institute, Hainan University, Haikou, People's Republic of China

*These authors contributed equally to this work

Correspondence: Miao Wang; Feifan Zhou, Email wangm@hainanu.edu.cn; zhouff@hainanu.edu.cn

Purpose: To avoid the biotoxicity and poor bioavailability of deferoxamine mesylate (DFO), an iron chelation for the treatment of Parkinson's disease (PD), a self-oriented DFO nanoparticle functionalized with Exendin-4 was developed, which can be targeted delivered into the lesion brain area to achieve synergistic effects against PD by iron chelation and inflammatory suppression.

Methods: The self-oriented DFO nanoparticles (Ex-4@DFO NPs) were synthesized by double emulsion technique, and characterized in terms of the particle size, morphology and DFO encapsulation efficiency. The cellular internalization, biocompatibility and cytoprotection of NPs were assessed on BV-2 and SH-SY5Y cells. The brain targeting and therapeutic effect of NPs were investigated in MPTP-induced PD mice by near-infrared II fluorescence imaging and immunofluorescence staining, as well as mobility behavioral tests.

Results: Ex-4@DFO NPs with a particle size of about 100 nm, showed great biocompatibility and cytoprotection in vitro, which inhibited the decrease of mitochondrial membrane potential of SH-SY5Y cells and the release of inflammatory factors of BV-2 cells. In MPTP-induced PD mice, Ex-4@DFO NPs could penetrate the BBB into brain, and significantly mitigate the loss of dopaminergic neurons and inflammation in the substantia nigra, finally alleviate the mobility deficits.

Conclusion: This self-oriented nanosystem not only improved the biocompatibility of DFO, but also enhanced therapeutic effects synergistically by ameliorating neuronal damage and neuroinflammation, showing a potential therapeutic strategy for PD.

Keywords: Parkinson's disease, deferoxamine mesylate, Exendin-4, nanoparticle system, brain targeting

Introduction

Parkinson's disease (PD) ranks as the second most common neurodegenerative disease, with the early degeneration of dopaminergic neurons in the substantia nigra pars compacta (SNc) as the main pathological feature.[1,2] The consequent dopamine shortage in the basal ganglia results in characteristic parkinsonian mobility deficits. Many studies have shown that alleviating glial cell-dominated inflammatory microenvironment and neuronal damage is helpful for the treatment of PD.[3,4] And substantial evidence indicates the presence of iron accumulation in both neurons and microglial cells within the SNc in PD.[5–8] The deposition of iron facilitates the generation of detrimental hydroxyl radicals during dopamine autooxidation, as well as triggers microglial activation and neuroinflammation, ultimately resulting in neuronal apoptosis.[9–12] These findings imply that iron-induced damage may be a crucial contributing factor to dopaminergic neurodegeneration and neuroinflammation.

Currently, the major clinical management of PD involves pharmacological therapy (primarily dopaminergic agents) and surgical intervention (such as deep brain stimulation, DBS).[13] Iron chelation therapy might be a promising pharmacological treatment by removing excess iron from the brain for neuroprotection.[14,15] Among the iron chelators currently employed in clinical practice for refractory anemia, deferoxamine mesylate (DFO) was demonstrated to be tolerated and highly effective to improve the patient life quality.[16,17] Several animal studies have indicated that DFO can

Received: 24 May 2024
Accepted: 30 September 2024
Published: 15 October 2024

Graphical Abstract

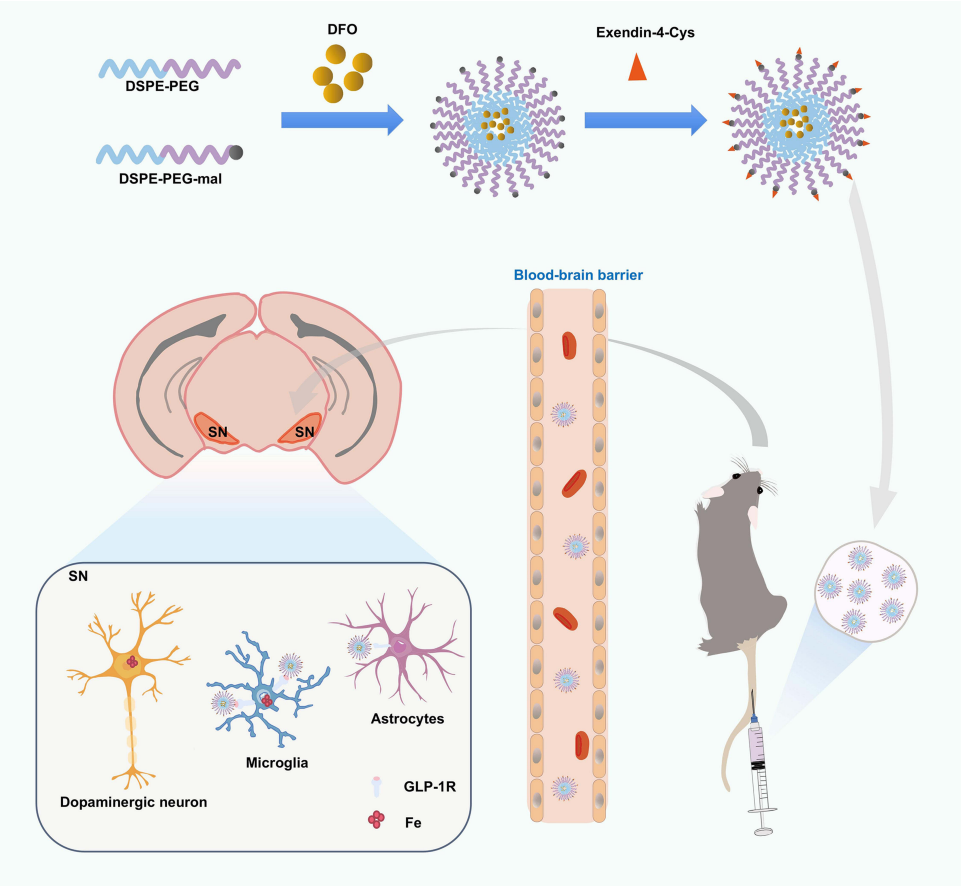

effectively inhibit dopaminergic neurodegeneration and resist nigrostriatal damage in PD models induced by MPTP or 6-OHDA.[18,19] However, due to its limited bioavailability, poor penetration of the blood-brain barrier (BBB), as well as biotoxicity at high doses, efficient and safe brain targeting transport of DFO has become a major challenge for application.[16,17,20,21]

Recent years have seen a rising interest in brain-targeted drug delivery systems, such as nanoparticle approaches, as a potential strategy for treatment by bypassing or traversing the BBB. Intranasal administration of dopamine-loaded nanoparticles enables their direct transport to the brain by circumventing the BBB.[22] The combination of DFO and rabies virus glycoprotein 29 (RVG) peptide facilitates the crossing of the BBB and enables targeting to neurons.[21] Glucagon-like peptide-1 receptor agonist (GLP-1RA), a novel agent used in the treatment of type 2 diabetes, which is demonstrated BBB-crossing potential.[23] Meanwhile, it is considered as a brain-targeting ligand, specifically binding to GLP-1R, which is abundantly expressed in the substantia nigra (especially on microglia) under PD pathological conditions.[24] Exendin-4, a type of GLP-1RA, has also shown neuroprotection for neurological diseases by promoting the survival and growth of neurons, maintaining the normal shape and function of synapses, and resisting oxidative stress, which was demonstrated potential in ameliorating motor function of PD patients during a clinical trial.[25–28]

In this study, we delicately designed and synthesized an Exendin-4 peptide-conjugated DFO-loaded nanoparticle system (Ex-4@DFO NPs) to target brain effectively for PD treatment. With the modification of brain-targeted molecular Exendin-4, Ex-4@DFO NPs improved the biocompatibility of DFO and increased the targeting to SNc in MPTP-induced PD mice. With the dual neuroprotective effects of Exendin-4 and DFO, Ex-4@DFO NPs more efficiently ameliorated

neurobehavioral deficits, neuronal loss, and neuroinflammation. The excellent alleviation efficacies on neuron damage and microglia activation by Ex-4@DFO NPs were verified in vitro and in vivo. The targeted iron chelator therapy based on multifunctional nanomaterials in this work probably offers a novel approach to treating PD.

Materials and Methods

Material

DSPE-PEG_{2000}, DSPE-PEG_{2000}-Mal, and DSPE-PEG_{2000}-FITC were obtained from Ponsure Biotechnology (China). The deferoxamine mesylate (DFO) was purchased from Sigma (USA). The Exendin-4 (Ex-4-Cys) peptide was purchased from Sangon Biotech (China).

Preparation of Nanoparticles (NPs)

The DP-DFO NPs were synthesized using a double emulsion technique. In brief, DSPE-PEG_{2000} (4.5 mg) and DSPE-PEG_{2000}-Mal (0.5 mg) were dissolved in methylene chloride (1 ml), followed by 0.2 ml aqueous solution of DFO (or water) addition. The mixture was sonicated for 3 min, and then was combined with 4 ml water and sonicated for 5 min, followed by standing at room temperature (RT) for 20 min. The product was vacuum evaporated at 30°C for methylene chloride removal. Finally, the NPs were harvested after the solution centrifuged (5000 g) for 15 min in ultrafiltration filters (3K MWCO (molecular weight cut-off)).

Ex-4-Cys was linked to the aforementioned NPs by a maleimide−thiol reaction between DSPE-PEG_{2000}-Mal and Ex-4-Cys. The NPs were incubated with Ex-4-Cys in water at RT for 24 h. Finally, the NPs were harvested after the solution centrifuged (5000 g) in ultrafiltration filters (10K MWCO) for unconjugated peptide removal.

NP Size, Zeta Potential and Micromorphology Measurement

Distribution of particle size and zeta potential of the nanoparticles were determined by dynamic light scattering (Zetasizer Nano ZSE, UK) at 25°C. The morphology of NPs was characterized by transmission electron microscopy (TEM). The diluted NPs suspension was dropped on a TEM grid and air-dried, followed by phosphotungstic acid staining for 30 s. Subsequently, the copper mesh was placed under a transmission electron microscope (Tecnai G2 Spirit, FEI, USA).

DFO Encapsulation Efficiency (EE) Measurement

The supernatant of Ex-4@DFO NPs was collected and reacted with excess $FeCl_3$ at RT for 1 h. The absorbance spectrum of DFO-Fe was detected by a UV spectrophotometer to estimate amount of free DFO. EE = (B - A)/B × 100%, where A represents the amount of free DFO in the supernatant, and B represents the amount of total DFO.

Matrix Assisted Laser Desorption Ionization-Time of Flight (MALDI–TOF) Mass Spectrometry

The conjugation of DSPE-PEG-MAL to Exendin-4 was determined by MALDI–TOF mass spectrometer (Bremen, Germany) equipped with a 337 nm nitrogen laser. The mass spectrum was acquired in linear and positive-ion modes, applying an acceleration voltage of 20 kV. A saturated mixture of sinapinic acid in acetonitrile:water (50:50, v–v) containing 0.1% TFA was utilized as a matrix solution. After mixing each analyte with the matrix solution in a 1:1 ratio, the samples were dried at RT.[23]

Measurement of Conjugation Efficiency (CE) of Exendin-4 Polypeptide

The supernatant of Ex-4@DFO NPs was collected and the concentration of free Exendin-4 peptide was assessed by high-performance liquid chromatography (HPLC).[23] The gradient program employed a C_{18} column with a mobile phase consisting of 0.1% trifluoroacetic acid in water (mobile phase A) and 0.1% trifluoroacetic acid in 80% acetonitrile (mobile phase B). 10 µl of each sample was injected and the elution process was monitored at 220 nm. The CE of

Exendin-4 was calculated as CE (%) = $(E_0 - E_1)/E_0 \times 100\%$, where E_0 represents the amount of total Exendin-4 peptide, and E_1 represents the amount of free Exendin-4 peptide in the supernatant of Ex-4@DFO NPs.

Cell Culture

BV-2 and SH-SY5Y cells (GuangZhou Jennio Biotech Co.,Ltd, China) were cultured in Dulbecco's Modified Eagle Medium (DMEM, Gibco, USA), supplied with 10% FBS (Gibco), penicillin (50 U/ml, Gibco) and streptomycin (50 mg/ml, Sigma), and kept in a sterile and humid condition (37°C, 5% CO_2).

Cell Viability Assay

BV-2 and SH-SY5Y cells were cultured in 96-well plates (1×10^4 cells/well) for 12 h and treated with various concentrations of drugs (0, 50, 100, 200 μM) for 24 h, respectively. Then the cell viability was assessed using cell counting kit-8 (CCK-8, Dojindo, Japan).

Intracellular Tracking of NPs

BV-2 and SH-SY5Y cells were cultured in 24-well plates respectively (1×10^5 cells/well) for 12 h. The FITC-functionalized Ex-4@DFO NPs were then co-incubated with BV-2 and SH-SY5Y cells for 8 h. Then the cells were incubated with the lysosome indicator Lyso-Tracker Red (Invitrogen, USA) for 30 min, followed by 10-min nuclear dye Hoechst 33342 (Invitrogen) staining. The cells were imaged by a confocal laser scanning microscope (CLSM, FV3000, OLYMPUS, Japan) to show cellular internalization of NPs.

Mitochondrial Membrane Potential Measurement

JC-1 fluorescence probe (Invitrogen) was used to measure the mitochondrial membrane potential of cells. SH-SY5Y cells were cultured in a 24-well plate (2×10^5 cells/well), then incubated with MPP+ (500 mm, MedChemExpress, NJ, USA) for 24 h, and then incubated with NPs for 2 h, followed by JC-1 staining for 20 min. The fluorescence images were acquired by CLSM (FV3000, OLYMPUS).

Intracellular ROS measurement

2′,7′-Dichlorofluorescin diacetate (DCFH-DA) probe (Invitrogen) was used to measure the generation of reactive oxygen radicals (ROS). SH-SY5Y cells were seeded in a 24-well plate (2×10^5 cells/well), cultured with MPP+ (500 mm) for 2 h, and then incubated with NPs for 2 h, followed by DCFH-DA staining for 30 min. The fluorescence images were collected using a fluorescence microscope (MD43-N, Mshot, China).

Animal Studies

Mice were purchased from Guangdong Medical Laboratory Animal Center. Male C57BL/6 mice (8–10 weeks, approximately 22–25 g) were used in the experiments. Mice were housed in a controlled environment with appropriate temperature and humidity, 12 h light and dark cycles, and given unrestricted access to standard diet and water. The mice treatments were performed in compliance with the Guide for the Care and Use of Laboratory Animals. All animal studies were reviewed and approved by the Institutional Animal Care and Use Committee of Hainan University (approval number: HNUAUCC-2021-00025).

Establishment and Treatment of Parkinson's Disease (PD) Mouse Models

The mice were habituated for a week, and the mice demonstrated equivalent performance in the rotating rod pre-training were selected for further studies. Firstly, mice underwent intraperitoneal injection of MPTP solution (30 mg/kg, Sigma) for 10 days to establish PD mouse models, while the mice in the control group received injections of the equivalent volume of normal saline. Simultaneously, for the investigation of NPs therapeutic effects for PD, the mice received intravenous injections of NPs solutions through the tail vein, starting from the first day of MPTP injection. These injections were administered at one-day intervals for a total of 6 times. Mice were sacrificed after all behavioral tests.

Rotarod Test

Rotarod test was conducted on an adjustable-speed rotarod (with a 3 cm diameter rod). Before the test, the mice were habituated in the test room for 30 min. Mice performed three 5-minute training sessions on the rotarod at a speed of 10 rpm/min to acclimate for three consecutive days before the formal test. A week after the treatments, the mice were subjected to an accelerating rotarod test. The speed of the rotarod was gradually increased from 4 to 40 rpm/min over 5 min, and latency to fall was recorded at each time using Visutrack software (Xinruan Information Technology Co., Ltd., China). The mice were tested 3 times per day, and the average latency to fall was taken as the final score.[29]

Open Field (OF) Test

Mice were placed in an open field apparatus (25 × 25 × 25 cm) and given 10 min to freely explore around. Total distance traveled (mm) and average velocity (mm/s) were recorded and analyzed using DigBehv behavior analysis system (Jiliang Software Science & Technology Co., Ltd., China).

In Vivo Distribution of NPs in the Mouse Brain

The PD mouse models established following the aforementioned protocol were administered with intravenous injection of DP-ICG NPs and Ex-4@ICG NPs. After 8 h, the mice were anesthetized and the scalp was removed, following which the distribution of NPs in the mouse brain was visualized using the MARS in vivo imaging system (Artemis Intelligent Imaging, China).

Blood Glucose Measurement

The hypoglycemic effect of NPs drugs was estimated on mice. A drop of blood was collected from tail vein during the six days of NPs administration, and blood glucose level was determined by a one-touch glucometer.

Tissue Collection and Immunofluorescence

The mice received intracardiac perfusion with PBS and 4% paraformaldehyde (PFA), and their entire brains were collected and fixed in PFA at 4°C for 24 h. Subsequently, the brains were dehydrated using sucrose solutions, and then were embedded in OCT (SAKURA, USA) and frozen at −80°C. The consecutive coronal brain sections (50 μm) were harvested. Then the slices were blocked with PBS containing 0.3% Triton X-100 (Sigma) and 5% bovine serum albumin (BSA, Sigma) at RT for 1 h. The brain sections were stained with rabbit anti-ionized calcium-binding adaptor up-regulated protein 1 (Iba1) antibody (cat# 019–19741, lot# LEN4341, 1:500, Fujifilm Wako) or mouse anti-tyrosine hydroxylase (TH) antibody (cat# MAB318, lot# 3858181, 1:1000, Sigma) dilutions at 4°C for 12 h, and stained with Alexa Fluor 555 anti-mouse IgG (H+L) secondary antibodies (cat# A21422, lot# 2418520, 1:500, Invitrogen) or Alexa Fluor 488 goat anti-rabbit IgG (H+L) secondary antibody (cat# A-32731, lot# VG302077, 1:500, Invitrogen) at RT for 1 h. The brain sections were imaged by CLSM (FV3000, OLYMPUS). The dopaminergic neuron number and microglia morphology in the SNc were analyzed and quantified using ImageJ.

RNA Isolation and Quantitative Real-Time PCR (qRT-PCR)

RNA of brain tissues was extracted with TRIzol reagent (Invitrogen). cDNA was generated using PrimeScrip RT Reagent Kit with gDNA (RR047A, TAKARA). QRT-PCR was performed on a Real-Time PCR Thermal Cycler (qTOWER, Analytik Jena) with TB Green Premix Ex Taq II (RR820A, TAKARA). Sequences of all primers are listed as follows: GAPDH: 5′-CAACTCACTCAA-GATTGTCAGCAA, 3′-GGCATGGACTGTGGTCATGA; TNF-α: 5′-CCAGT GTGGGAAGCTGTCTT, 3′-AAGCAAAAGAGGAGGCAACA.

Statistical Analysis

Statistical significance was conducted using two-tailed unpaired Student's *t*-test for two-group comparisons, and one-way ANOVA with Sidak's multiple comparison test or two-way ANOVA with Sidak's multiple comparison test for multiple-group

comparisons. A P value less than 0.05 was considered statistically significant (*$P < 0.05$, **$P < 0.01$ and ***$P < 0.001$). Data are presented as mean ± SEM. Statistical data were analyzed using GraphPad Prism (GraphPad Software, Inc.).

Results

Characterization of Ex-4@DFO NPs

The polymeric NPs were fabricated with the well-known biodegradable substance DSPE-PEG, which is extensively utilized for delivery systems.[30] The hydrophilic DFO was contained within the hydrophilic core, which was synthesized by a double emulsion technique. Then the brain-targeting molecule Exendin-4 was covalently attached to the DFO-loaded NPs by reacting the thiol groups with maleimide groups on the NPs surface.

The morphology and surface charge of the nanoparticles were assessed by dynamic light scattering (DLS). The average particle sizes of DP-DFO, DP-Ex-4 and Ex-4@DFO NPs were about 100 nm, and the zeta potentials of DP-DFO and Ex-4@DFO NPs detected as −45.4 ± 2.6 mV and −47.3 ± 1.8 mV, respectively (Figure 1A–D). The results demonstrated that the size and surface charge of the NPs exhibited minimal changes after Exendin-4 conjugation. Additionally, the polydispersity index (PDI) value reflects the uniformity of nanomaterial products. The average PDI values of DP-DFO and Ex-4@DFO NPs were 0.219 ± 0.003 and 0.208 ± 0.010, respectively. The low PDI value suggested the uniform size distribution of the NPs. Moreover, transmission electron microscopy (TEM) images further confirmed the uniform spherical morphology of Ex-4@DFO NPs (Figure 1B).

DFO can combine with ferric ions at a molar ratio of 1:1 to form a non-toxic and stable chelate DFO-Fe. For the determination of encapsulation efficiency (EE) of DFO, the supernatant of Ex-4@DFO NPs was collected and reacted with $FeCl_3$ solution, and the UV absorption spectra of DFO-Fe were measured to calculate the amount of free DFO in the supernatant. The results showed no UV absorption of DFO alone in the detection wavelength range, while the characteristic absorption peak of the Fe^{3+} was observed at around 300 nm (Figure 1E). Differently, DFO-Fe compounds presented a distinct absorption peak at approximately 430 nm (Figure 1F). Standard curve of DFO-Fe concentration versus absorbance was shown in Figure 1G. Based on the absorbance curve of DFO-Fe in the mixture of supernatant of Ex-4@DFO NPs with $FeCl_3$ solution, the DFO encapsulation efficiency of Ex-4@DFO NPs was calculated as 35.5 ± 0.5%, indicating that DFO has been successfully encapsulated into the NPs.

To verify the successful conjugation of Exendin-4 to DP-DFO NPs, the reaction product of Exendin-4 polypeptide and DSPE-PEG-MAL was determined by Matrix assisted laser desorption ionization-time of flight mass spectrometry (MALDI–TOF MS). As shown in Figure 1H and I, the specific peaks for Exendin-4 (4290 m/z) and DSPE-PEG-MAL (2900 m/z) were observed in the respective samples, respectively. In the reaction product, a peak at 6900 m/z revealed covalent linkage between Exendin-4 polypeptide and DSPE-PEG-MAL (Figure 1J). For determination of the conjugation efficiency of Exendin-4, the supernatant of Ex-4@DFO NPs was detected by high-performance liquid chromatography (HPLC), and the content of free Exendin-4 was quantified using the standard curve of Exendin-4 (Figure 1K). The conjugation efficiency of Exendin-4 polypeptide to DP-DFO NPs was calculated as 94%.

Biological Impact and Cytoprotection Effects of NPs

To determine the cellular internalization and distribution of the NPs, BV-2 and SH-SY5Y cells were incubated with FITC-functionalized Ex-4@DFO (Ex-4@DFO-FITC) NPs for a duration of 12 h, and cultured with Lyso-Tracker Red for lysosome staining, respectively. The results showed that the fluorescence signal of Ex-4@DFO-FITC NPs was predominantly localized within the cells, particularly in the lysosomes. These findings suggested that Ex-4@DFO NPs possess the ability of cellular internalization and accumulation in both two types of cells, particularly in the lysosomes (Figure 2A).

To investigate the biocompatibility of NPs on BV-2 and SH-SY5Y cells, the cells were treated with the NPs (0, 50, 100, 200 μM), and the cell viability was assessed by CCK-8 assay. The results demonstrated that both DFO and DP-DFO NPs induced remarkable cellular damage to SH-SY5Y cells at 50 μM. In contrast, there was no damage to cells with the treatment of Ex-4@DFO NPs up to 100 μM (Figure 2B).

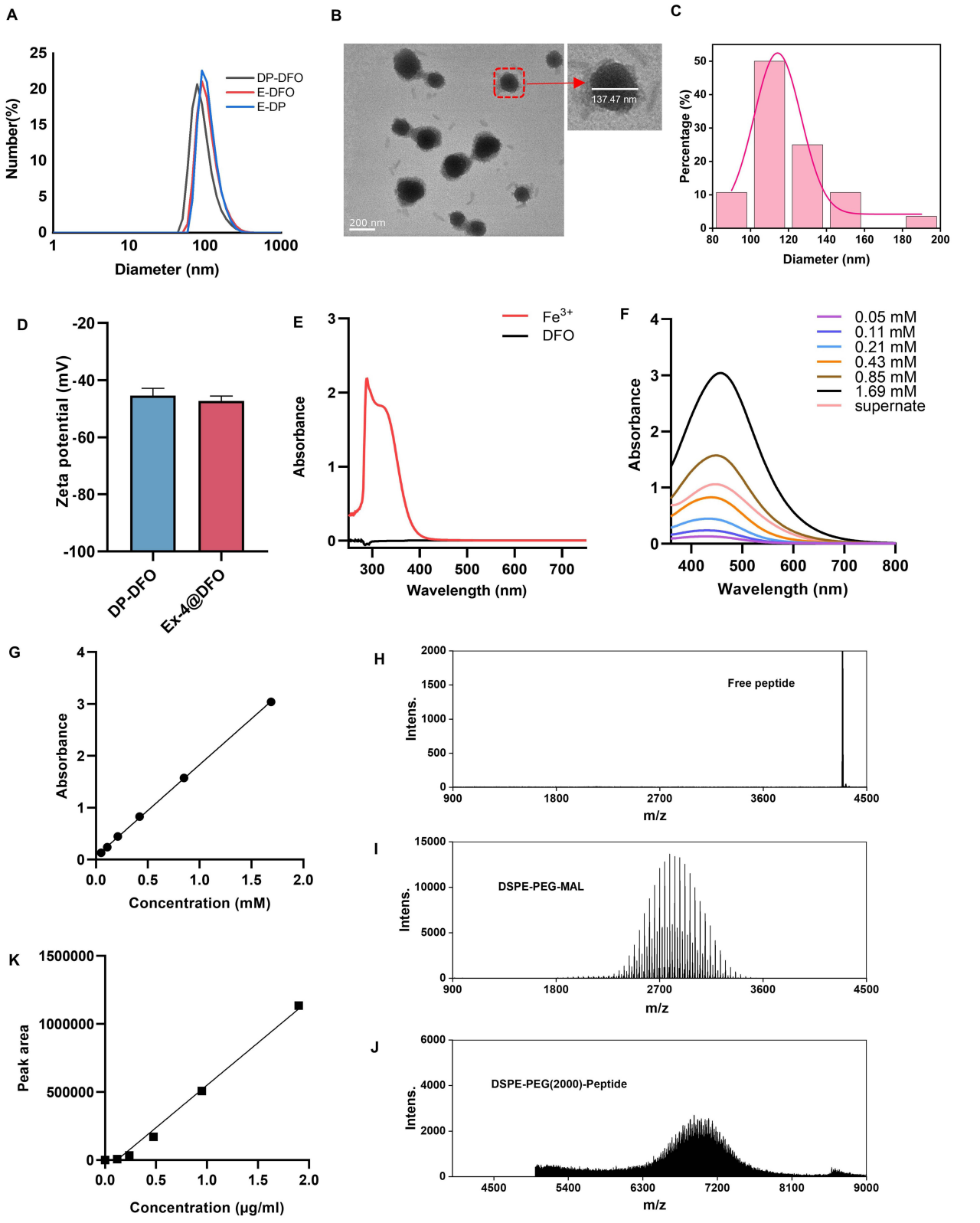

Figure 1 Characterization of the nanoparticles. (**A**) Size distribution of Ex-DP, DP-DFO and Ex-4@DFO NPs assessed by dynamic light scattering (DLS). (**B**) Representative transmission electron microscopy (TEM) images of Ex-4@DFO NPs. Scale bar = 200 nm. (**C**) Size distribution of Ex-4@DFO NPs assessed by TEM. (**D**) Zeta potential of DP-DFO and Ex-4@DFO NPs (n = 3). (**E**) UV-Vis absorption spectrum of DFO solution and Fe^{3+} solution. (**F**) UV-Vis absorption spectra of DFO-Fe with different concentrations. (**G**) Standard curve of DFO-Fe. (**H–J**) The mass spectra of Exendin-4 (**H**), DSPE-PEG-MAL (**I**), DSPE-PEG-Ex-4 (**J**). m/z: mass to charge ratio. (**K**) Standard curve of Exendin-4. Data are presented as mean ± SEM.

https://doi.org/10.2147/IJN.S479670 DovePress

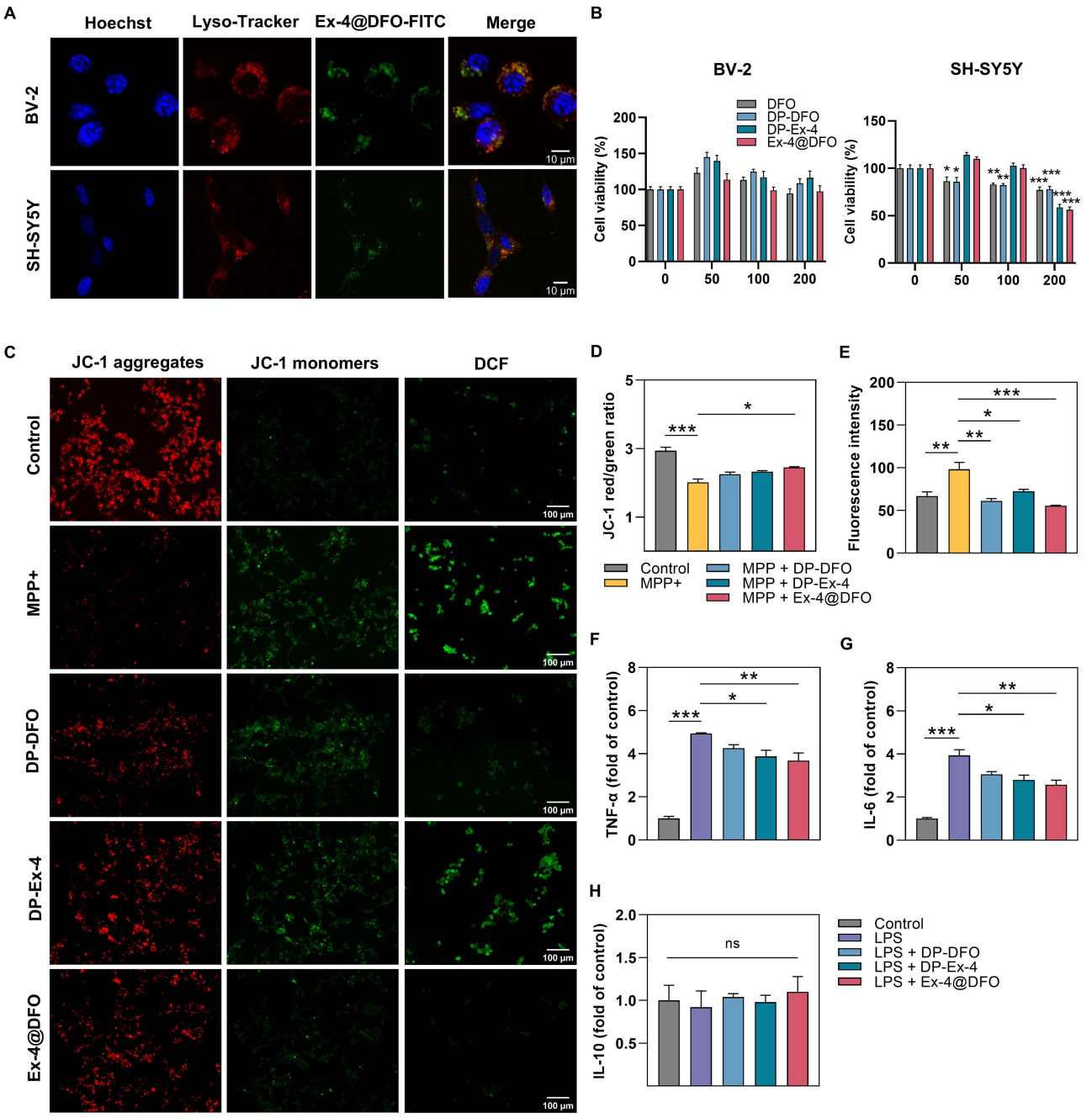

Figure 2 Biological effects of the nanoparticles on BV-2 and SH-SY5Y cells. (**A**) Representative cellular internalization fluorescence images of SH-SY5Y cells after incubation with Ex-4@DFO-FITC NPs for 8 h. Scale bar = 10 μm. (**B**) Cytotoxicity of different nanoparticles toward BV-2 and SH-SY5Y cells (n = 5). (**C**) Representative fluorescence images of treated SH-SY5Y cells incubated with JC-1 probe (mitochondrial membrane potential indicator) and 2′,7′-dichlorofluorescin diacetate (DCFH-DA) probe (reactive oxygen radicals (ROS) indicator). DCF fluorescence is generated from the oxidization of nonfluorescent DCFH-DA by ROS. Scale bar = 100 μm. (**D**) Quantification of the mitochondrial membrane potential in treated SH-SY5Y cells measured by the red/green fluorescence ratio of JC-1 (n = 3). (**E**) Quantification of the fluorescence intensity of DCFH in treated SH-SY5Y cells (n = 3). (**F**–**H**) Expression of proinflammatory cytokine TNF-α (**F**), IL-6 (**G**) and anti-inflammatory cytokine IL-10 (**H**) from treated BV-2 cells determined by Elisa kits (n = 3). Data are presented as mean ± SEM. **P* < 0.05, ***P* < 0.01, ****P* < 0.001 as assessed by two-way ANOVA with Sidak's multiple comparison test for comparisons of multiple groups (**B**), or one-way ANOVA with Sidak's multiple comparison test for comparisons of multiple groups (**D**–**H**).

Decrease in mitochondrial membrane potential and excessive production of reactive oxygen species (ROS) may imply mitochondrial dysfunction and lead to cell apoptosis.[10] To explore the neurological effects of Ex-4@DFO NPs in PD, SH-SY5Y cells were incubated with MPP+ (500 mm) for establishment of PD cell model, followed by treatments with the NPs (100 μM) for 2 h, and the mitochondrial membrane potential and ROS generation were assessed using JC-1

probe and 2′,7′-dichlorofluorescin diacetate (DCFH-DA) probe. The results showed that the fluorescence ratio of JC-1 polymer red to green decreased in MPP+-treated SH-SY5Y cells, indicating reduction of mitochondrial membrane potential, while Ex-4@DFO NPs treatment inhibited the decrease of mitochondrial membrane potential. Additionally, the fluorescence intensity of 2',7'-dichlorofluorescein (DCF, produced by oxidation of DCFH-DA by ROS) was elevated in the MPP+ group compared to the control group. In contrast, all three types of NPs reduced fluorescence signals. These findings suggested that MPP+ induced ROS production in neurons and the NPs downregulated the ROS levels, revealing that Ex-4@DFO NPs, DP-DFO NPs and DP-Ex-4 NPs had the ability to scavenge ROS (Figure 2C–E). Overall, both Ex-4@DFO and DP-Ex-4 NPs inhibited the increase of ROS, but only Ex-4@DFO NPs inhibited the decrease of mitochondrial membrane potential, which indicated the abnormalities of the mitochondrial function. Subsequently, for determination of the cytoprotection impact of NPs, the effect of inflammatory inhibition on microglia was assessed. BV-2 cells were exposed with LPS (100 ng/ml) to induce cellular inflammation, and then treated with different types of NPs for 2 h. Then cell culture supernatant from different treatments were collected and analyzed using tumor necrosis factor-α (TNF-α), interleukin-6 (IL-6), and interleukin-10 (IL-10) ELISA Kits. The result demonstrated that Ex-4@DFO and DP-Ex-4 NPs downregulated secretion of TNF-α and IL-6 elicited by LPS, while no significant effects on IL-10 levels (Figure 2F–H). Therefore, both Ex-4@DFO and DP-Ex-4 NPs inhibited the increase of inflammatory factors in vitro.

Inflammation affects mitochondrial function and further lead to cell death in Parkinson's disease. The inflammatory processes trigger a chain of events including increased production of ROS, disruption of iron metabolism and mitochondrial dysfunction, generating a self-feeding cycle that could lead to neurodegeneration in diseases.[31] DFO, a kind of iron chelators, can efficiently decrease the cellular iron content and be helpful for mitochondrial iron homeostasis.[32] Exendin-4 can inhibit the higher production of ROS in neuronal cells,[33] and prevent neural apoptosis and mitochondrial dysfunction through several cellular signal pathways, such as GLP-1 receptor/Epac/Akt signaling pathway.[34,35] DFO and Exendin-4 may play cytoprotective roles by regulating the level of iron and ROS, respectively. The results demonstrated that Ex-4@DFO NPs inhibited the decrease of mitochondrial membrane potential, and the production of ROS generation, and inhibited the increase of inflammatory factors in vitro, which showed more efficient amelioration than DP-Ex-4 and DP-DFO NPs.

Brain Targeting and Biocompatibility of NPs

To verify the ability of ex-conjugated fluorescent NPs of the BBB penetration and brain targeting in vivo, MPTP-induced PD mice were intravenously injected with DP-ICG or Ex-4@ICG NPs. After 8 h, the mice were sacrificed for brain collection to ex vivo assess the NPs accumulation. As shown in Figure 3A and B, a higher fluorescence intensity was observed in the brain in Ex-4@ICG NPs group compared to DP-ICG NPs group, showing greater accumulation of Ex-4-conjugated NPs. The result indicated that Ex-4-conjugated NPs could penetrate the BBB as well as deliver drugs to brain.

Additionally, to explore in vivo cytotoxicity of NPs, histopathological analysis of major organs was further performed after NPs administration to mice. The H&E-stained images indicated that all the NPs had no significant tissue damage to the major organs of mice (Figure 3C). These results demonstrated that the Ex-4@DFO NPs held brain targeting and good biocompatibility.

Restoration of Functional Disorders in PD Mice by Ex-4@DFO NPs Treatment

To investigate the in vivo therapeutic effect of NPs, the MPTP-induced PD mouse models were established and verified by mobility behavior tests. Before the treatments, mice underwent a three-day pre-training, and the mice with stable behavior were chosen for further tests. The mice were intraperitoneally injected with MPTP solution for 10 consecutive days for PD model establishment. Simultaneously, the treatment drugs DP-DFO, DP-Ex-4 (Exendin-4 polypeptide content 1 μg/kg) and Ex-4@DFO NPs (DFO content 35 mg/kg) were administrated intravenously to mice every other day for a total of 6 times. Five days after the treatments, efficacy on mobility of mice was then evaluated using rotarod test and open field (OF) test (Figure 4A). PD mice exhibited distinctly reduced residence time on rotarod compared to control mice. However, treatment with Ex-4@DFO NPs increased the time spent on rotarod of PD mice, identical to that of control mice, while neither DP-DFO nor DP-EX-4 NPs treatment showed significant improvement (Figure 4B). Furthermore, NPs treatments did not exhibit changes in total distance and average speed in the OF test in PD

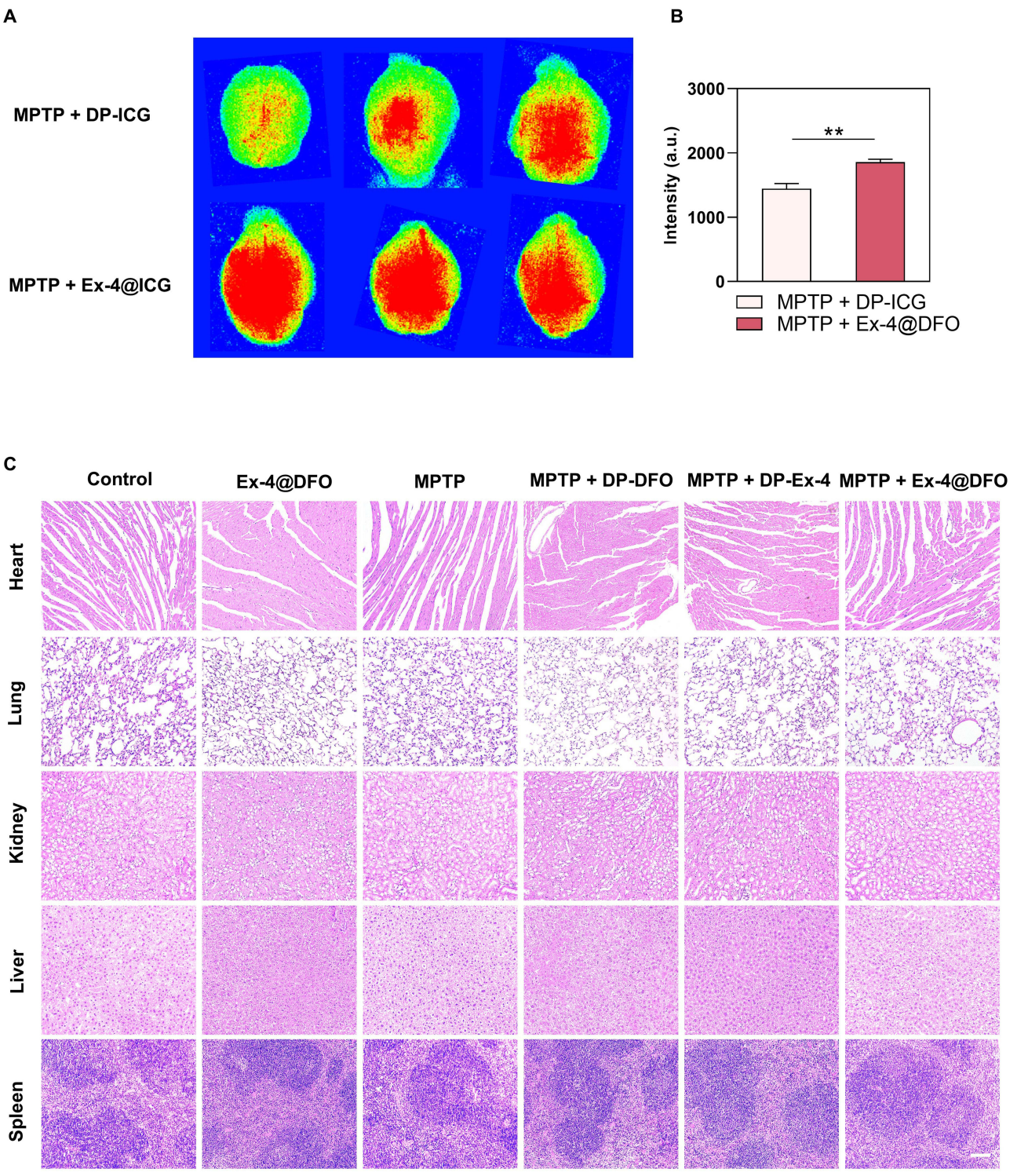

Figure 3 In vivo brain targeting and biocompatibility of Ex-4@DFO NPs. (**A**) Ex vivo fluorescence images of the brain from PD mice intravenously treated with DP-ICG or Ex-4@ICG NPs for 8 h (n = 3). (**B**) Average fluorescence intensities at the brain sites quantified 8 h post injection (n = 3). (**C**) Representative H&E-stained section images of the major organs 8 h post intravenous injection of NPs (n = 3). Scale bar = 100 μm. Data are presented as mean ± SEM. $^{**}P < 0.01$ as assessed by two-tailed unpaired Student's *t*-test for two-group comparisons (**B**).

mice (Figure 4C and 4D). In addition, no distinct changes in body weight or blood glucose levels were observed in any of the groups during the treatment period (Figure 4E and F). The results indicated that Ex-4@DFO NPs were biocompatible and effectively improved PD-related motor deficits.

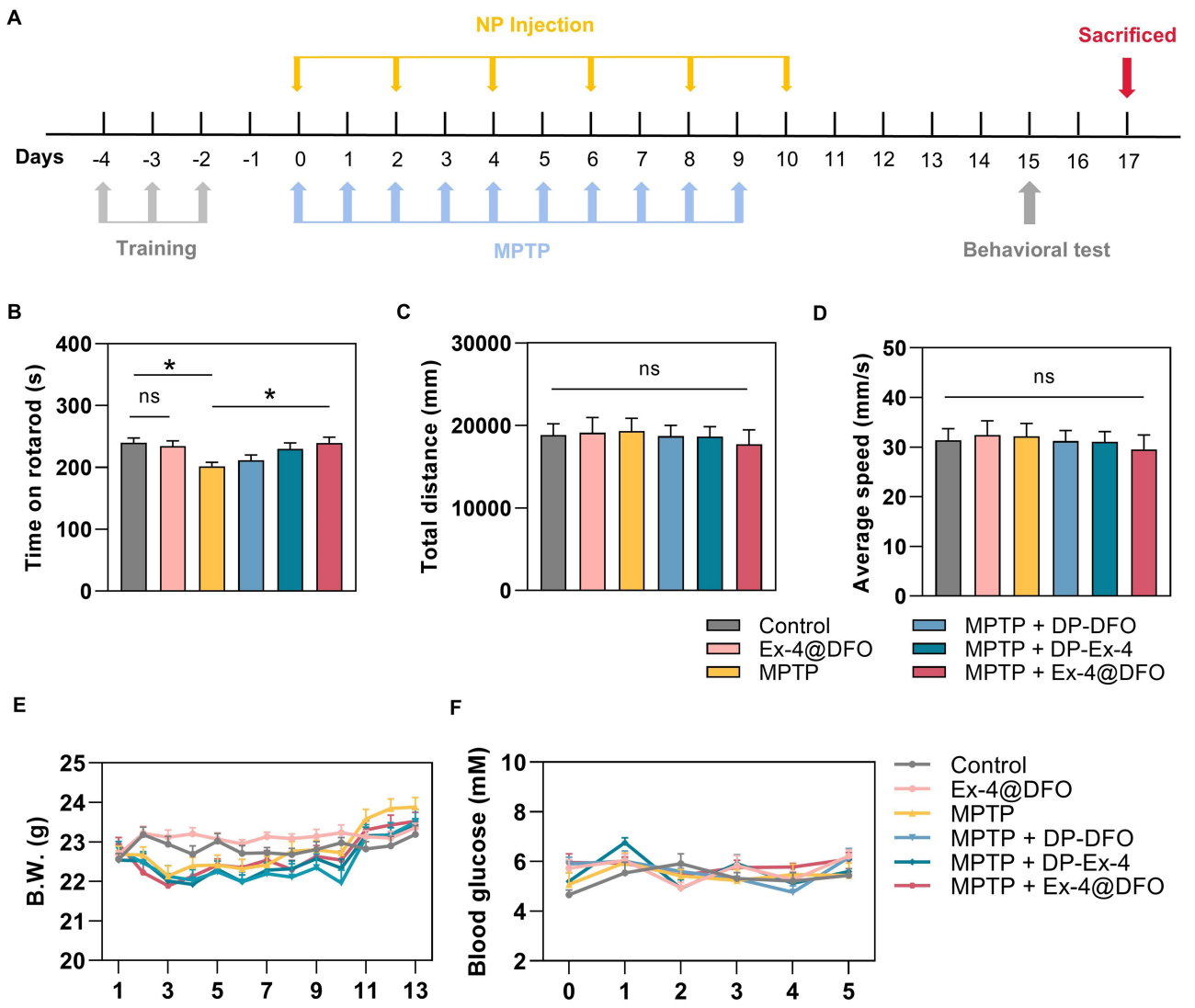

Figure 4 Improvement effects of Ex-4@DFO NPs on PD-related motility disorders in mice. (**A**) Schedule of establishment of PD mouse model, NPs treatments and behavioral tests of mice. (**B**) Time on rotarod of mice in rotarod test (n = 11 in MPTP + DP-DFO group; n = 10 in other groups). (**C** and **D**) Total traveled distance (**C**) and average speed (**D**) in open field test (n = 11 in MPTP + DP-DFO group; n = 10 in other groups). (**E**) Changes of body weight (B.W.) of different treated mice (n = 10 in Control, Ex-4@DFO, MPTP + DP-Ex-4, MPTP + Ex-4@DFO groups; n = 9 in MPTP group; n = 11 in MPTP + DP-DFO group). (**F**) Changes of blood glucose of different treated mice (n = 5). Data are presented as mean ± SEM. *$P < 0.05$ as assessed by one-way ANOVA with Sidak's multiple comparison test for comparisons of multiple groups (**B**–**D**), or two-way ANOVA with Sidak's multiple comparison test for comparisons of multiple groups (**E** and **F**).

To further reveal neurological efficacy of NPs, the alterations in dopaminergic neuronal damage and inflammation in the SNc were analyzed. Tyrosine hydroxylase (TH) is a key enzyme involved in neurotransmitter synthesis, whose expression is closely associated with the functionality of dopaminergic neurons. The decline in TH expression is considered to be an indicator of dopaminergic neuron damage. Therefore, brain sections were immunostained with TH antibody. As depicted in Figure 5A and C, the TH level in the SNc of PD mice was lower than that of control mice. However, TH expression increased after Ex-4@DFO NPs treatment. In contrast, neither DP-DFO nor DP-Ex-4 NPs showed any inhibitory effect on neuronal damage. The result indicated that Ex-4@DFO NPs alleviated dopaminergic neuronal damage in PD mice.

Chronic neuroinflammation is one of the pathophysiological hallmarks of PD. Usually, activated microglia chronically release pro-inflammatory cytokines, leading to increased dopaminergic neuron degeneration. The morphological characteristics of microglia, such as branch length and branch number of microglia could show their activation status. To investigate whether Ex-4@DFO NPs can reduce microglia activation and relieve neuroinflammation in MPTP-induced

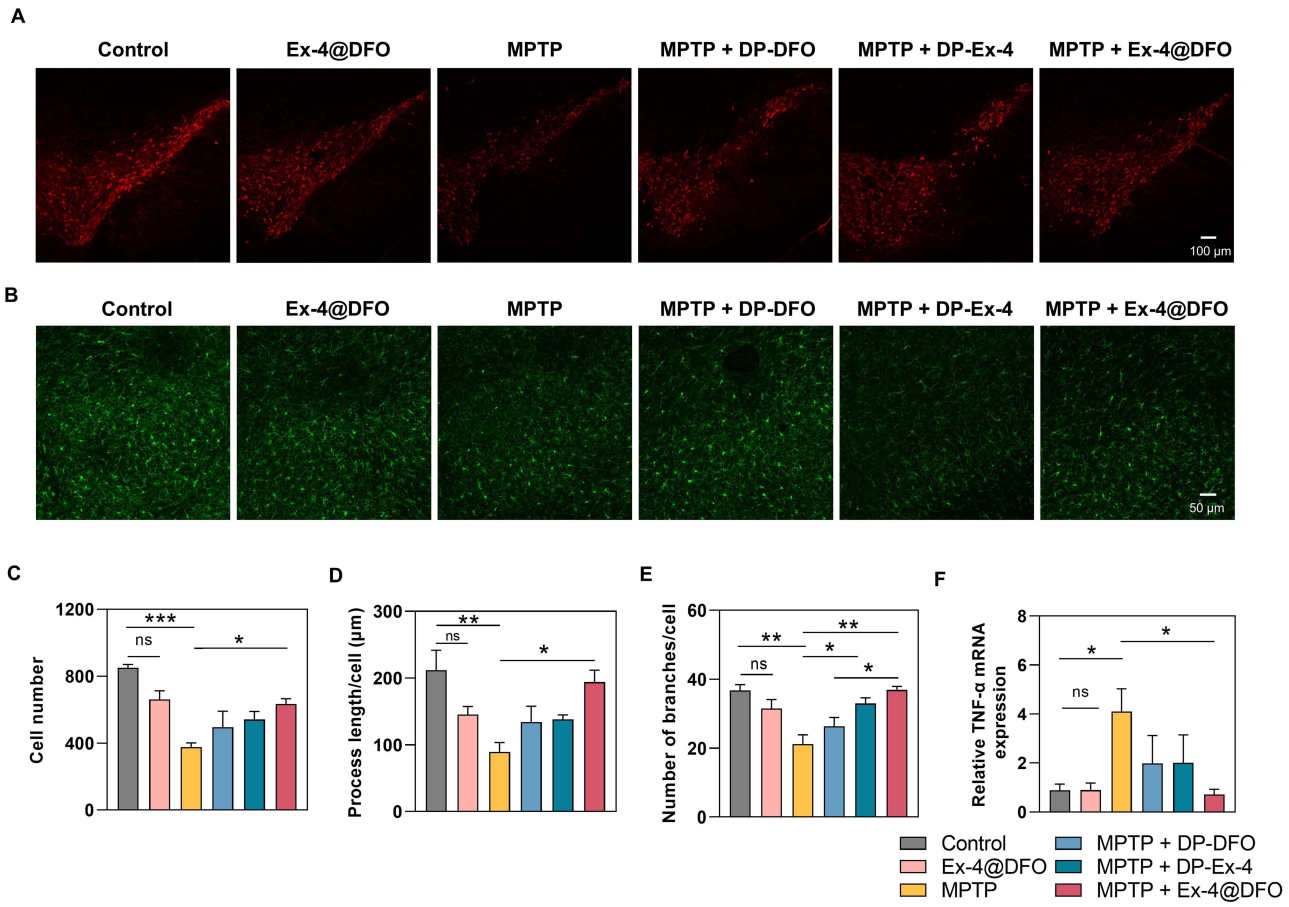

Figure 5 Improvement effects of Ex-4@DFO NPs on PD-related neurological damage and neuroinflammation in mice. (**A** and **B**) Representative images of brain sections in the substantia nigra pars compacta (SNc) stained with tyrosine hydroxylase (TH) (**A**) or Iba1 (**B**) antibody. Scale bar = 100 μm or 50 μm. (**C**) Quantification of the number of TH^+ neurons in the SNc (n = 3). (**D** and **E**) Quantification of branch length per cell (**D**) and number of branches per cell (**E**) of $Iba1^+$ cells (n = 3). (**F**) Quantification of expression of TNF-α mRNA in the SNc of mice (n = 3). Data are presented as mean ± SEM. **P* < 0.05, ***P* < 0.01, ****P* < 0.001 as assessed by one-way ANOVA with Sidak's multiple comparison test for comparisons of multiple groups (**C–F**).

mice, the SNc brain sections were immunostained with ionized calcium-binding adaptor up-regulated protein 1 (Iba1) antibody for morphological analysis of microglia, and TNF-α expression in the SNc was assessed by quantitative polymerase chain reaction (qPCR). The results revealed that MPTP treatment induced a phenotypic activation of microglia showing the reduction in branch length and branch number. In contrast, microglia in Ex-4@DFO NPs-treated PD mice presented longer branch and more branch number (Figure 5B, D and E). In addition, qPCR analysis showed that there was a distinct elevation of TNF-α level in SNc of PD mice, while decreased in Ex-4@DFO NPs-treated PD mice (Figure 5F). These findings demonstrated that Ex-4@DFO NPs treatment restored the neuroinflammation in PD mice.

Conclusion

In this study, a biocompatible NP functionalized with SNc-targeting neuroprotective peptide Exendin-4 was developed to transport the iron chelator DFO to brain for synergetic PD amelioration. The Ex-4@DFO nanosystem was found to be efficiently internalized in both microglia and neuron cells in vitro. Both Ex-4@DFO and DP-Ex-4 NPs demonstrated the properties of cytoprotection effect and inflammation suppression in vitro. Moreover, only Ex-4@DFO NPs administration effectively rescued the neurological and neuroinflammatory damage in SNc, and ameliorated the PD-related mobility deficits.

All the results indicated that the self-oriented of targeted molecular Exendin-4 to SNc, the lesion area of PD mice, ensured targeting drug delivery and therapeutic effect. In addition, the Exendin-4 modification not only improved the biocompatibility of DFO, but also enhanced therapeutic effects synergistically by ameliorating neurobehavioral deficits,

neuronal loss, and neuroinflammation. Our findings suggest that this self-oriented nanocarrier might become a promising therapeutic strategy for PD treatment by synergistic effects of iron chelators and inflammatory suppression.

Data Availability Statement

The data that support the findings of this study are available from the corresponding author upon reasonable request.

Acknowledgments

F.Zhou, M.Wang, and F.Yue conceived and designed the experiments. Y.Huang, W.Li, and X.Wang performed the experiments and analyzed the data. Y.Huang, X.Wang, M.Wang, and F.Zhou wrote the manuscript. All the authors read and approved the manuscript.

Funding

This study was funded in part by the STI2030-Major Projects (2022ZD0212200, 2021ZD0200900); Hainan Province Key Area R&D Program (KJRC2023C30, ZDYF2021SHFZ094), and Project of Collaborative Innovation Center of One Health (XTCX2022JKB02, XTCX2022JKC05).

Disclosure

The authors declare no competing interests.

References

1. Poewe W, Seppi K, Tanner CM, et al. Parkinson disease. *Nat Rev Dis Primers*. 2017;3:17013. doi:10.1038/nrdp.2017.13
2. Kalia LV, Lang AE. Parkinson's disease. *Lancet*. 2015;386(9996):896–912. doi:10.1016/S0140-6736(14)61393-3
3. Li Q, Ding X, Chang Z, et al. Metal-organic framework based nanozyme system for NLRP3 inflammasome-mediated neuroinflammatory regulation in Parkinson's Disease. *Adv Healthc Mater*. 2024;13(10):e2303454. doi:10.1002/adhm.202303454
4. Li Q, Wu T, Akakuru OU, et al. A dual synergetic nanoreactor for managing Parkinson's disease by regulating inflammation and mitigating oxidative damage. *Adv Func Mat*. 2023;33(37):2214826. doi:10.1002/adfm.202214826
5. Castellani RJ, Siedlak SL, Perry G, Smith MA. Sequestration of iron by Lewy bodies in Parkinson's disease. *Acta Neuropathol*. 2000;100 (2):111–114. doi:10.1007/s004010050001
6. Dexter DT, Wells FR, Lees AJ, et al. Increased nigral iron content and alterations in other metal ions occurring in brain in Parkinson's disease. *J Neurochem*. 1989;52(6):1830–1836. doi:10.1111/j.1471-4159.1989.tb07264.x
7. Jellinger K, Paulus W, Grundke-Iqbal I, Riederer P, Youdim M. Brain iron and ferritin in Parkinson's and Alzheimer's diseases. *J Neural Trans-Parkinson's Dis Dementia Sect*. 1990;2:327–340. doi:10.1007/BF02252926
8. Morris C, Edwardson J. Iron histochemistry of the substantia nigra. *Neurodegeneration*. 1994;3:277–282.
9. Hare DJ, Double KL. Iron and dopamine: a toxic couple. *Brain*. 2016;139(4):1026–1035. doi:10.1093/brain/aww022
10. Liu H, Han Y, Wang T, et al. Targeting microglia for therapy of Parkinson's disease by using biomimetic ultrasmall nanoparticles. *J Am Chem Soc*. 2020;142(52):21730–21742. doi:10.1021/jacs.0c09390
11. Núñez González M, Urrutia PJ, Mena N, Aguirre P, Tapia V, Salazar J. Iron toxicity in neurodegeneration. *Biometals*. 2012;25:761–776. doi:10.1007/s10534-012-9523-0
12. Zhang K, Tu M, Gao W, et al. Hollow prussian blue nanozymes drive neuroprotection against ischemic stroke via attenuating oxidative stress, counteracting inflammation, and suppressing cell apoptosis. *Nano Lett*. 2019;19(5):2812–2823. doi:10.1021/acs.nanolett.8b04729
13. Armstrong MJ, Okun MS. Diagnosis and treatment of Parkinson disease: a review. *JAMA*. 2020;323(6):548–560. doi:10.1001/jama.2019.22360
14. Chen J, Marks E, Lai B, et al. Iron accumulates in Huntington's disease neurons: protection by deferoxamine. *PLoS One*. 2013;8(10):e77023. doi:10.1371/journal.pone.0077023
15. Lee JK, Shin JH, Gwag BJ, Choi EJ. Iron accumulation promotes TACE-mediated TNF-alpha secretion and neurodegeneration in a mouse model of ALS. *Neurobiol Dis*. 2015;80:63–69. doi:10.1016/j.nbd.2015.05.009
16. Bayanzay K, Alzoebie L. Reducing the iron burden and improving survival in transfusion-dependent thalassemia patients: current perspectives. *J Blood Med*. 2016;7:159–169. doi:10.2147/JBM.S61540
17. Shah J, Kurtin SE, Arnold L, Lindroos-Kolqvist P, Tinsley S. Management of transfusion-related iron overload in patients with myelodysplastic syndromes. *Clin J Oncol Nurs*. 2012;16 Suppl:37–46. doi:10.1188/12.CJON.S1.37-46
18. Aguirre P, Mena NP, Carrasco CM, et al. Iron chelators and antioxidants regenerate neuritic tree and nigrostriatal fibers of MPP+/MPTP-lesioned dopaminergic neurons. *PLoS One*. 2015;10(12):e0144848. doi:10.1371/journal.pone.0144848
19. Guo C, Hao LJ, Yang ZH, et al. Deferoxamine-mediated up-regulation of HIF-1alpha prevents dopaminergic neuronal death via the activation of MAPK family proteins in MPTP-treated mice. *Exp Neurol*. 2016;280:13–23. doi:10.1016/j.expneurol.2016.03.016
20. Lynch SG, Fonseca T, LeVine SM. A multiple course trial of desferrioxamine in chronic progressive multiple sclerosis. *Cell Mol Biol*. 2000;46 (4):865–869.
21. You L, Wang J, Liu T, et al. Targeted brain delivery of rabies virus glycoprotein 29-modified deferoxamine-loaded nanoparticles reverses functional deficits in parkinsonian mice. *ACS Nano*. 2018;12(5):4123–4139. doi:10.1021/acsnano.7b08172

22. Garcia-Pardo J, Novio F, Nador F, et al. Bioinspired theranostic coordination polymer nanoparticles for intranasal dopamine replacement in Parkinson's Disease. *ACS Nano*. 2021;15(5):8592–8609. doi:10.1021/acsnano.1c00453
23. Athauda D, Foltynie T. The glucagon-like peptide 1 (GLP) receptor as a therapeutic target in Parkinson's disease: mechanisms of action. *Drug Discov Today*. 2016;21(5):802–818. doi:10.1016/j.drudis.2016.01.013
24. Yun SP, Kam TI, Panicker N, et al. Block of A1 astrocyte conversion by microglia is neuroprotective in models of Parkinson's disease. *Nat Med*. 2018;24(7):931–938. doi:10.1038/s41591-018-0051-5
25. Athauda D, Maclagan K, Skene SS, et al. Exenatide once weekly versus placebo in Parkinson's disease: a randomised, double-blind, placebo-controlled trial. *Lancet*. 2017;390(10103):1664–1675. doi:10.1016/S0140-6736(17)31585-4
26. Bertilsson G, Patrone C, Zachrisson O, et al. Peptide hormone exendin-4 stimulates subventricular zone neurogenesis in the adult rodent brain and induces recovery in an animal model of Parkinson's disease. *J Neurosci Res*. 2008;86(2):326–338. doi:10.1002/jnr.21483
27. Kim S, Moon M, Park S. Exendin-4 protects dopaminergic neurons by inhibition of microglial activation and matrix metalloproteinase-3 expression in an animal model of Parkinson's disease. *J Endocrinol*. 2009;202(3):431–439. doi:10.1677/JOE-09-0132
28. Li Y, Perry T, Kindy MS, et al. GLP-1 receptor stimulation preserves primary cortical and dopaminergic neurons in cellular and rodent models of stroke and Parkinsonism. *Proc Natl Acad Sci U S A*. 2009;106(4):1285–1290. doi:10.1073/pnas.0806720106
29. Ma X, Hao J, Wu J, Li Y, Cai X, Zheng Y. Prussian blue nanozyme as a pyroptosis inhibitor alleviates neurodegeneration. *Adv Mater*. 2022;34(15):e2106723. doi:10.1002/adma.202106723
30. Che J, Okeke CI, Hu ZB, Xu J. DSPE-PEG: a distinctive component in drug delivery system. *Curr Pharm Des*. 2015;21(12):1598–1605. doi:10.2174/1381612821666150115144003
31. Urrutia PJ, Mena NP, Nunez MT. The interplay between iron accumulation, mitochondrial dysfunction, and inflammation during the execution step of neurodegenerative disorders review. *Front Pharmacol*. 2014;5. doi:10.3389/fphar.2014.00038
32. Zheng Q, Zhao Y, Guo J, et al. Iron overload promotes mitochondrial fragmentation in mesenchymal stromal cells from myelodysplastic syndrome patients through activation of the AMPK/MFF/Drp1 pathway. *Cell Death Dis*. 2018;9(5):515. doi:10.1038/s41419-018-0552-7
33. Jo D, Yoon G, Song J. Role of Exendin-4 in brain insulin resistance, mitochondrial function, and neurite outgrowth in neurons under palmitic acid-induced oxidative stress. *Antioxidants*. 2021;10(1):78. doi:10.3390/antiox10010078
34. Garabadu D, Verma J. Exendin-4 attenuates brain mitochondrial toxicity through PI3K/Akt-dependent pathway in amyloid beta (1-42)-induced cognitive deficit rats. *Neurochem Int*. 2019;128:39–49. doi:10.1016/j.neuint.2019.04.006
35. Pandey S, Mangmool S, Madreiter-Sokolowski CT, Wichaiyo S, Luangmonkong T, Parichatikanond W. Exendin-4 protects against high glucose-induced mitochondrial dysfunction and oxidative stress in SH-SY5Y neuroblastoma cells through GLP-1 receptor/Epac/Akt signaling. *Eur J Pharmacol*. 2023;954:175896. doi:10.1016/j.ejphar.2023.175896